*Ab initio* and empirical studies on the asymmetry of molecular current–voltage characteristics



2007 J. Phys.: Condens. Matter 19 215206

(http://iopscience.iop.org/0953-8984/19/21/215206)

IOP PUBLISHING JOURNAL OF PHYSICS: CONDENSED MATTER

J. Phys.: Condens. Matter **19** (2007) 215206 (14pp) doi:10.1088/0953-8984/19/21/215206

# *Ab initio* and empirical studies on the asymmetry of molecular current–voltage characteristics

**R C Hoft, N Armstrong, M J Ford[1] and M B Cortie**

Institute for Nanoscale Technology, University of Technology Sydney, PO Box 123, Broadway NSW 2007, Australia

E-mail: mike.ford@uts.edu.au

Received 28 September 2006, in final form 19 January 2007
Published 1 May 2007
Online at stacks.iop.org/JPhysCM/19/215206

**Abstract**

We perform theoretical calculations of the tunnelling current through various small organic molecules sandwiched between gold electrodes by using both a tunnel barrier model and an *ab initio* transport code. The height of the tunnelling barrier is taken to be the work function of gold as modified by the adsorbed molecule and calculated from an *ab initio* electronic structure code. The current–voltage characteristics of these molecules are compared. Asymmetry is introduced into the system in two ways: an asymmetric molecule and a gap between the molecule and the right electrode. The latter is a realistic situation in scanning probe experiments. The asymmetry is also realized in the tunnel barrier model by two distinct work functions on the left and right electrodes. Significant asymmetry is observed in the *ab initio* $i(V)$ curves. The tunnel barrier $i(V)$ curves show much less pronounced asymmetry. The relative sizes of the currents through the molecules are compared. In addition, the performance of the WKB approximation is compared to the results obtained from the exact Schrödinger solution to the tunnelling barrier problem.

## 1. Introduction

The field of molecular electronics, originating from the gedanken experiment of Aviram and Ratner [1] who postulated a molecular rectifier consisting of a donor–acceptor molecule, is receiving a lot of interest due to ever-improving techniques for realizing larger scale systems consisting of single molecules as building blocks. On the theoretical side, much effort is being made to understand the transport of electrons through individual molecules. Due to the complexity of this problem, the focus is often on simpler molecules than the original proposal by Aviram and Ratner. Transport is thought to occur by resonant tunnelling when there are molecular energy levels in close range of the Fermi level. In molecules with very localized

[1] Author to whom any correspondence should be addressed.

  

orbitals, and hence large 'band gaps', non-resonant tunnelling is responsible for transport. In addition to understanding the mechanism of transport, phenomena such as asymmetric $i(V)$ curves and negative differential resistance are also of interest due to their possible exploitation in molecular electronic devices. It is now well established that the transport properties are not a function of the molecule alone, but rather of the electrode–molecule–electrode system as interface effects play a major role.

Density functional theory (DFT) [2, 3] has become a *de facto* standard for such transport calculations where a single molecule is sandwiched between metal electrodes and the system repeated periodically. Electronic structures are calculated self-consistently within DFT and then used in a non-equilibrium Green's function (NEGF) method for calculating transport properties. DFT currently provides the best trade-off between computational speed and reliability of results. Nevertheless, currents calculated with DFT–NEGF can be up to orders of magnitude larger than typical experimental currents [4], but efforts have been made to reconcile experimental and DFT results by including less than optimal bonding configurations in the theoretical investigations [5–9]. Recently it has been shown that dynamical effects not present in the static DFT approach can lead to corrections in the junction resistance, particularly for metal-organic molecule junctions where the charge distribution could vary rapidly across the junction [10–12].

In this paper we calculate and compare current–voltage characteristics of various small molecules sandwiched between Au(111) electrodes using both *ab initio* and empirical techniques and exact solutions to the barrier tunnelling problem. In particular we investigate the asymmetry in the $i(V)$ properties that results from the inherent asymmetry in a molecule as well as asymmetric contact conditions on the two electrodes.

We use a DFT–NEGF code to calculate the structure of the Au(111)–molecule–Au(111) systems under an applied bias between left and right electrodes. Here, the full electronic structure of the system plays a role in the nature of the transport, and resonant tunnelling may occur if molecular energy levels, i.e. the highest occupied molecular orbital (HOMO) or the lowest unoccupied molecular orbital (LUMO), lie close to the Fermi level of the system after shifting and broadening due to the interaction with the gold electrodes. Inclusion of dynamic effects as described by Sai *et al* [10] lies outside the scope of the present calculations.

An alternative viewpoint is to treat the transport problem as tunnelling across a potential barrier formed by the interelectrode region occupied by a molecule. In this model the important parameters are the height, shape and length of the tunnel barrier. The barrier height is taken to equal the work function of the Au(111) surface, modified by the adsorption of a monolayer of the particular molecule, and is calculated from first principles using DFT. Reduction of the work function of an electrode by surface layers is well known. For example, coating tungsten [13, 14] and other cathodes [14] with BaO can significantly reduce the cathode work function. In this case the reduction of the work function has been correlated with the density of Ba–O dipoles [14]. The shape of the barrier is taken to be a trapezoid, which can be modified by sinusoidal rounding at the interfaces to account for image charging.

We also consider the case where the molecule does not span the entire interelectrode distance, i.e. the molecule is bound to the left electrode, with a gap between the molecule and the right electrode. In this case we use a double trapezoidal barrier to account for different barrier heights in the different media.

Two methods have been developed to calculate the transmission function across this potential barrier. The first is the well-known Wentzel–Kramers–Brillouin (WKB) approximation for barrier tunnelling; the second is the exact solution to the Schrödinger equation for a single or double trapezoidal barrier. The WKB calculations also include barriers with and without interface rounding.

## 2. Method

### *2.1. Ab initio*

The minimum energy adsorption geometries of the molecules on the Au(111) surface are obtained with the DFT-based electronic structure code SIESTA which invokes periodic boundary conditions [15, 16]. This code employs a linear combination of numerical atom-centred basis functions for the valence electrons and norm-conserving pseudopotentials generated according to the scheme of Troullier and Martins [17] for the core electrons. The key feature of the code is that orbitals are strictly localized in space with a cutoff radius defined by an energy shift parameter for all atoms, being the energy increase of the orbitals due to the confinement. In our calculations this parameter is set to 5 mRyd. A Monkhorst–Pack grid [18] of $5 \times 5$ $k$-points in the plane of the surface is used. Only one $k$-point is needed perpendicular to the slab, since there is no periodicity in this direction. For each atom, double-$\zeta$ plus polarization orbitals are included in the basis. The unit cell consists of four gold layers with $3 \times 3$ Au atoms per layer and one adsorbed molecule. This ensures that the molecule is sufficiently separated from its periodic images to avoid any intermolecular interactions. We have previously determined that this set of parameters provides well-converged equilibrium geometries and interaction energies for similar systems [19]. The exchange–correlation energy is calculated with the generalized gradient approximation, as parametrized by Perdew, Burke and Ernzerhof [20]. A mixture of $Z$-matrix and Cartesian input coordinates are used to define the structure and geometry optimizations performed within these mixed coordinates. This is particularly convenient for studying the surface adsorption of molecules [21].

For the calculation of the work functions, these parameters are varied to find a set of parameters that yield accurate work functions (see section 3.1 below). The work function is calculated as the difference between the Fermi level of the surface plus adsorbed molecule and the electrostatic potential far away from the surface

$$\phi = V_\infty - E_\mathrm{F}. \tag{1}$$

The transport calculations are performed with TranSIESTA-C, a commercial version of an extension of the SIESTA package. This package uses NEGFs together with the density matrix to obtain the current through an electrode–molecule–electrode system with an applied bias between electrodes [22]. These calculations can be computationally expensive, and thus an unrelaxed set of parameters is used. This will affect the absolute values but does not alter the qualitative behaviour or trends in the calculated currents. While the molecular atoms are represented by double-$\zeta$ plus polarization orbitals, we include only single-$\zeta$ plus polarization orbitals for the gold atoms. The energy shift parameter is set to 10 mRyd and only the $\Gamma$-point is used in sampling the $k$-space parallel to the surface. Exchange–correlation energies are calculated using the local density approximation, parametrized by Perdew and Zunger [23].

### *2.2. The WKB approximation*

The WKB approximation is widely used to approximate the transmission function for an arbitrary barrier shape. Using this approximation, the transmission function between two electron reservoirs at distance $d$ apart with a particular barrier function can be written as

$$T(E, V, d) = \exp\left(-\frac{2\sqrt{2}}{\hbar}\int_0^d \mathrm{d}x\sqrt{m\,[U(x) - E]}\right) \tag{2}$$

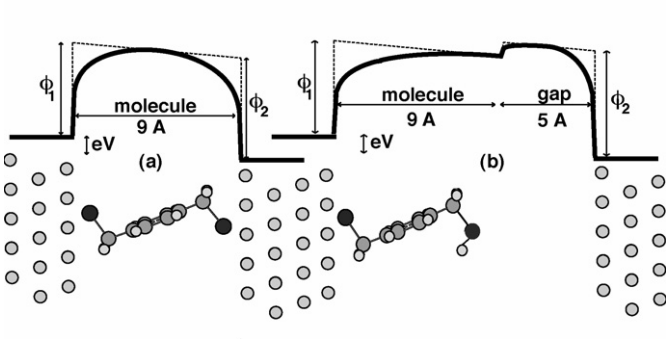


**Figure 1.** Barrier shapes $U(x)$ used in the WKB approximation and Schrödinger calculations. (a) Trapezoidal barrier used for a molecule that spans the intermolecular distance. For a symmetric molecule $\phi_1 = \phi_2$. (b) A double trapezoidal barrier representing a molecule attached to the left electrode with a gap between the other end and the right electrode. Here $\phi_1$ is the work function of the surface with the adsorbed molecule (left) and $\phi_2$ is the work function of the bare surface (right). Solid lines indicate rounded barrier shapes (i.e. $\alpha > 0$), while dashed lines indicate shapes with no rounding ($\alpha = 0$).

where $m$ is the mass of an electron and $U(x)$ is the barrier function between the reservoirs. The corresponding current can be expressed as [24]

$$i(V,d) = \frac{2e}{h}\int_{-\infty}^{\infty} \mathrm{d}E \cdot T(E,V,d) \cdot \rho_1(E-eV)\rho_2(E) \cdot \left[f(E) - f(E-eV)\right] \tag{3}$$

where $\rho_1$ and $\rho_2$ are the density of states, $f(E)$ and $f(E-eV)$ are the Fermi functions of the two electrodes and $eV$ is the bias potential between the two electrodes. The contact conductance is taken to be the quantum of conductance $2e/h = 77\ \mu\mathrm{S}$. This relation is simplified by assuming a constant density of states and zero temperature

$$i(V,d) = \frac{2e}{h}\int_{0}^{eV} \mathrm{d}E \cdot \exp\left(-\frac{2\sqrt{2}}{\hbar}\int_{0}^{d} \mathrm{d}x\sqrt{m\left[U(x)-E\right]}\right). \tag{4}$$

The present calculation assumes a rounded trapezoidal barrier shape given by

$$U(x) = eV\left(1-\frac{x}{d}\right) + \left[\phi_1 + \frac{x}{d}(\phi_2-\phi_1)\right] \cdot \left[\sin\left(\frac{\pi x}{d}\right)\right]^{\alpha}, \tag{5}$$

where $\phi_1$ and $\phi_2$ are the left and right surface work functions, respectively; and $\alpha$ is the rounding parameter, chosen to be 0.2 [25]. For $\alpha = 0$, equation (5) reduces to a trapezoid with 'sharp' interfaces as shown in figure 1(a).

A double trapezoid barrier model is used to describe the case where a vacuum gap exists between an adsorbed molecule and the right electrode (see figure 1(b)). This model describes two barriers in series through which the electrons tunnel. At the boundary between the two trapezoids, continuity is achieved by applying the same sinusoidal rounding to both trapezoids.

### *2.3. Schrödinger equation barrier calculations*

The transmission probability and current were also determined using the full Schrödinger equation. As with the WKB approximation, a trapezoidal barrier model was assumed, but with 'sharp' edges, i.e. $\alpha = 0$ in (5). We have solved the Schrödinger equation exactly for both the single and double trapezoidal models. Due to the complexity and length of the solutions, it is impractical to present them here. However, we will provide an outline of the solution for a single trapezoidal barrier model.

As pointed out above, taking (5) and setting $\alpha = 0$ defines a trapezoidal barrier for $0 \leqslant x \leqslant d$ with sharp edges. The corresponding solutions are given by

$$u(x) = \begin{cases} Ae^{ik_1 x} + Be^{-ik_1 x}, & x < 0 \\ CAi(\eta) + DBi(\eta) & 0 \leqslant x \leqslant d \\ Ge^{ik_3 x}, & x > d \end{cases} \tag{6}$$

where $A$, $B$, $C$, $D$ and $G$ are the transmission coefficients; $k_1 = k_3 = k$, such that

$$k = \sqrt{\frac{2mE}{\hbar^2}}.$$

The functions $Ai(\eta)$ and $Bi(\eta)$ in (6) are Airy functions, where $\eta$ is defined as

$$\eta = \left(\frac{2m}{\hbar^2 d}(eV - \phi_1 + \phi_2)\right)^{1/3} \left[\frac{eV + \phi_1 - E}{eV - \phi_1 + \phi_2} - x\right]. \tag{7}$$

In order to determine the transmission function, the continuity condition for each solution in (6) must satisfy the boundaries of the barrier. Following on from this, the corresponding set of equations can be solved, and the transmission function of the incident and final waves can be expressed in terms of $A$ and $G$ coefficients,

$$T(E, U_b, \phi_1, \phi_2, d) = \left|\frac{G * G}{A * A}\right| \tag{8}$$

where the '$*$' represents the complex conjugate of the coefficient. The solution for the double barrier follows the same methodology, but requires an additional set of boundary conditions that must be matched.

In developing the exact solutions for the single and double barrier, the only assumption that has been made is that the shape of the barrier is known *a priori*. Moreover, by exploring the exact solutions for both cases, this ensures that the properties of the barriers and transmission currents can be understood, from which reliable inferences about desirable characteristics of the absorbing molecules can be made. That is, the WKB approximation is reliable for thick barriers or in the 'far-field', where $(d/\hbar)\sqrt{2m[U(x) - E]} \gg 1$ [26]. In determining the exact transmission function for both cases, we have not been able to explore the effect that rounded barriers have on the transmissions currents.

## 3. Results and discussion

### *3.1. Adsorbing molecules*

The various molecules sandwiched between the Au(111) surfaces are shown in figure 2. When the molecule adsorbs on the Au(111) surface it is assumed that the terminal hydrogen is removed to form a strong chemisorbed bond on the surface. Our previous calculations predicted this bond to be stronger than the thiol bond when the hydrogen atom is kept in place [9]. Although the nature of the bond (thiolate versus thiol) has not been unambiguously determined, there is considerable evidence favouring the thiolate case assumed here [27]. We have also previously confirmed that the ethynylbenzene molecule, the single-ended version of figure 2(b), is likely to chemisorb in a similar fashion by losing the terminal hydrogen atom and forming stable SAMs (self-assembled monolayer) [19]. Our calculated interaction energy for the ethynylbenzene molecule is larger than for thiol-linked molecules such as 1,4-benzenedimenthanethiol (XYL). This, together with the unbroken conjugation extending through the C–C triple bonds in diethynylbenzene (DEB) directly to the gold surface, may lead to the molecule having a higher conductance than its thiol-linked counterpart.

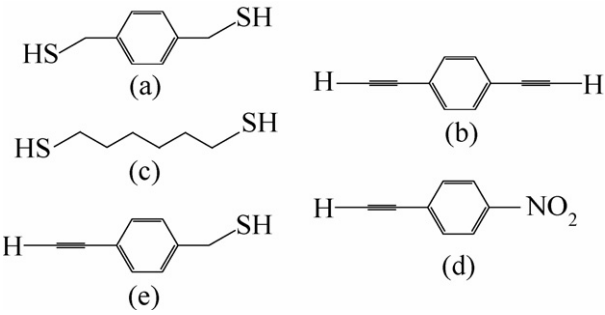


**Figure 2.** (a) 1,4-benzenedimenthanethiol (XYL), (b) diethynylbenzene (DEB), (c) hexanedithiol (C6), (d) 1-ethynyl-4-nitrobenzene (ENB) and (e) 1,4-ethynylphenylmethanethiol (EPM). EPM and ENB are the only asymmetric molecules.

We calculated the optimum position of the sulfur-terminated molecules 2(a), 2(c) and 2(e) to be 2.0 Å above the surface, between the fcc and bridge sites. The terminating carbon on molecules 2(b), 2(d) and 2(e) is positioned 1.3 Å above the surface in the fcc site.

The adsorbing molecules XYL, hexanedithiol (C6), DEB and 1,4-ethynylphenylmethane - thiol (EPM) were placed between Au(111) electrodes with the interface geometries on each side determined by the respective adsorption geometries, as in figure 1(a). The adsorption geometry of the $NO_2$ group in molecule 2(d) was not determined in this work and hence we do not present an $i(V)$ curve for 1-ethynyl-4-nitrobenzene (ENB) in this geometry. Instead, the ethynyl side is attached to the left Au(111) electrode and a gap of 5 Å is present between the $NO_2$ and the right electrode, as in figure 1(b). The same molecule–gap geometry is used with the other molecules in figure 2. Since EPM is asymmetric this yields two possible geometries. We refer to the case where the thiol end is bound to the left electrode as EPM-S and where the ethynyl end is bound to the left electrode as EPM-C. Note that at the interface with the 5 Å gap the terminal hydrogen atom is retained, since there is no chemical bond between the molecule and electrode on this side.

### *3.2. Calculation of the surface energy and work function*

In order to test our calculations we have calculated the surface energy of Au(111) as well as the work functions. Obtaining accurate computational results for the surface properties of metals is not an easy task as evidenced by the large spread in theoretical values obtained for surface energies and interlayer relaxation in the literature [28–31].

In calculating the properties of the bare Au(111) surface it is only necessary to use one Au atom per surface layer. This is repeated periodically to represent the surface. We therefore need a denser $k$-point grid for accurate $k$-space sampling. We present in figure 3(a) our most computationally intensive results for the surface energy of Au(111), where we have used $19 \times 19$ $k$-points in the plane parallel to the surface and an energy shift parameter of 0.1 mRyd. We use an independently calculated single-atom bulk energy $E_{bulk}$ to calculate the surface energy $E_S(n)$ of slabs with total energy $E_n$ represented by increasing numbers of layers $n$ from

$$E_S(n) = \tfrac{1}{2}\,(E_n - n \cdot E_{\text{bulk}})\,. \tag{9}$$

We found the alternative method proposed by Boettger [32] for estimating the bulk energy as the difference in energy between slabs of increasing thickness to produce larger variation in $E_S(n)$. We find $E_S(n) = 0.31$ eV/atom or 41 meV Å$^{-2}$. The results are shown in figure 3(a).

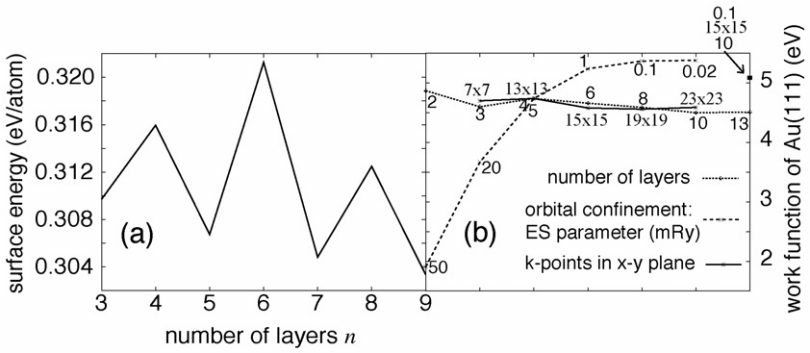


**Figure 3.** (a) The Au(111) surface energy obtained with an increasing number of slab layers to estimate the surface using (9). (b) Convergence of the calculated work function of the bare Au(111) surface with respect to the number of layers used to estimate the slab, the orbital confinement parameter and the number of $k$-points used in the plane parallel to the surface.

**Table 1.** Work functions of Au(111) with adsorbed molecules.

| Adsorbed molecule | $\phi$ (eV) |
|---|---|
| Bare Au(111) | 5.13 |
| XYL | 4.92 |
| C6 | 4.90 |
| EPM-S | 4.91 |
| EPM-C | 4.50 |
| DEB | 4.31 |
| ENB | 5.77 |

The best experimental value of ∼96 meV Å$^{-2}$ [33] is much larger, but this is an extrapolation of high-temperature data and is averaged over the faces of polycrystalline gold. It may be expected that the (111) surface has lower energy. Crljen *et al* [31] and Yourdshayan *et al* [29] both found $E_S \sim 50$ meV Å$^{-2}$ using plane wave DFT and the generalized gradient approximation (GGA).

Figure 3(b) shows our calculations of the surface work function of a bare Au(111) slab. We test for convergence with respect to the number of slab layers used to approximate the surface, the orbital confinement (energy shift) parameter and the number of $k$-points used in the plane parallel to the surface. The convergence is carried out independently for each parameter, as the cost of increasing the computational load associated with all three parameters simultaneously is prohibitive. The common set of parameters is indicated where the three curves in figure 3(b) cross, i.e. using four layers, a 5 mRyd cutoff and 13 × 13 $k$-points. One parameter at a time is then changed while keeping the other two fixed at these values. We find the parameter values at which the work function is well-converged to be 10 layers, 0.1 mRyd cutoff and 15 × 15 $k$-points. Repeating the calculation with these three parameters used simultaneously yields a work function $\phi_{Au} = 5.13$ eV compared with the experimental value of 5.31 eV using the photoelectric effect [34]. Notably, the work function is very sensitive to a relaxation of the orbital confinement energy, whereas the number of slab layers and $k$-point sampling does not have as large an effect. Our calculated value is in reasonable agreement with the experiment.

In order to calculate the work function of the Au(111) slab with adsorbed molecules, 3 × 3 Au atoms per slab layer are needed to ensure that the molecules do not interact with their periodic neighbours. The number of $k$-points used is 5 × 5, which corresponds exactly to 15 × 15 $k$-points for the primitive cell. The results are summarized in table 1. Clearly, all

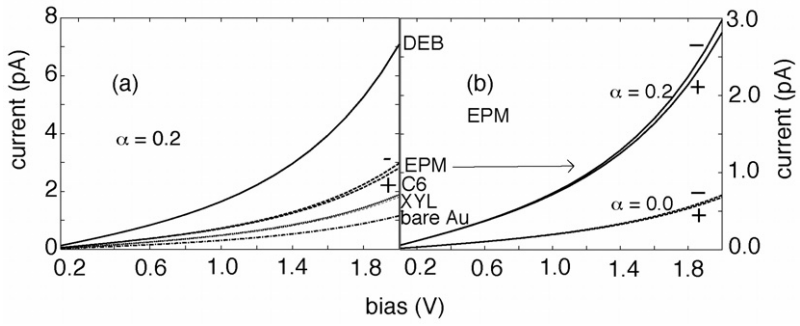


**Figure 4.** (a) $i(V)$ curves calculated using the WKB approximation, equation (4), for various molecules spanning the interelectrode distance of 9 Å. (b) Comparison of the forward and reverse bias currents of EPM using a rounded and 'sharp' trapezoidal barrier.

but the ENB molecule act to reduce the surface work function. EPM-S and EPM-C refer to the EPM molecule attached to the Au(111) surface on the thiol and ethynyl sides, respectively. The effect of the adsorbed molecules is largely dominated by the nature of the bond coupling it to the surface, except for the ENB molecule that has a large intrinsic dipole moment. The gold–carbon bond in the case of DEB and EPM-C is more effective than the gold–sulfur bond at reducing the work function.

### *3.3. i(V) curves using the tunnel barrier model*

The model described in section 2.2 was applied to calculate $i(V)$ curves for each of the molecules. A single trapezoidal barrier was first considered and corresponds to the molecule spanning the interelectrode region. The barrier length was set to be 9 Å. This length defines the approximate length of the molecules shown in figure 2. The transmission current was calculated using both the WKB approximation (4) and solving the Schrödinger equation exactly. The barrier heights are taken from table 1. Figure 4(a) shows WKB $i(V)$ curves using the sinusoidally rounded ($\alpha = 0.2$) trapezoidal barrier.

The asymmetry in the $i(V)$ curve for the inherently asymmetric molecule EPM is shown in figures 4(a) and (b). The positive current is slightly smaller than the negative current, where the positive current corresponds to electrons flowing from left to right in figure 1. The EPM molecule was aligned between the electrodes with the ethynyl side attached to the left electrode, so that the barrier height is lower on the left (4.50 eV) than on the right (4.91 eV). By studying equation (4), we can show that the greater electron flow will always be from the side with larger barrier height to the side with smaller barrier height. This is true for both the single and double trapezoid cases. Of course this result only holds when the applied bias is less than the barrier height; outside this regime the WKB approximation itself breaks down.

Figure 4(b) shows how the size and asymmetry changes when the barrier is not rounded. Evidently, the size of the current decreases substantially for sharp barriers, since there is a larger area to integrate under the barrier. The asymmetry at 2 V bias is about 4% for the sharp barrier and 6% for the rounded barrier.

Figure 5(a) shows a similar comparison between the $i(V)$ curves of the various molecules with a 5 Å gap between the molecule and right electrode. The interfaces at the electrodes and at the step are rounded as shown in figure 1(b). Consistent with the above discussion, the forward bias currents (i.e. electrons tunnelling from left to right) are smaller for the molecules that decrease the surface work function due a larger barrier height on the right. For the ENB

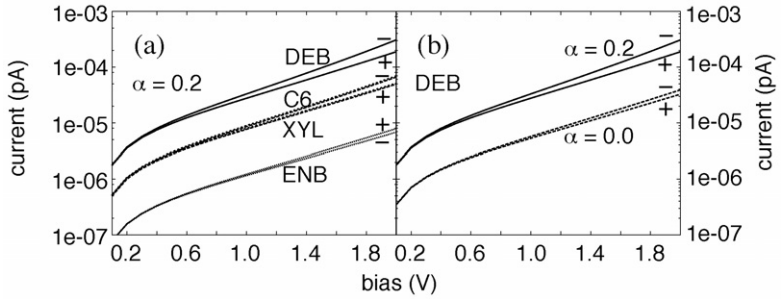


**Figure 5.** (a) $i(V)$ curves calculated using the WKB approximation, equation (4), for various molecules with a 5 Å gap between the molecule and right electrode. (b) Comparison of the forward and reverse bias currents of DEB using a rounded and non-rounded stepwise trapezoidal barrier.

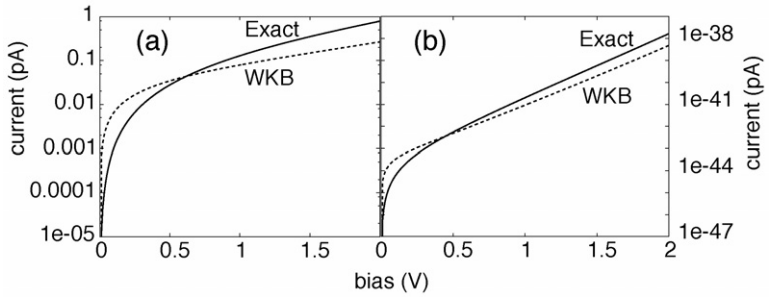


**Figure 6.** Exact and WKB $i(V)$ curves for a single trapezoidal barrier consisting of bare Au using different barrier lengths, $d$: (a) $i(V)$ curves for $d = 9$ Å; (b) $i(V)$ curves for $d = 50$ Å.

molecule, that increases the barrier height, the forward bias current is larger. Figure 5(b) compares the size and asymmetry of the DEB $i(V)$ curve in this case with a rounded and sharp barrier. Again the rounding increases the current substantially and enhances the asymmetry. At a 2 V bias the excess reverse bias current over forward bias current is 60% for the rounded barrier and only 20% for a sharp barrier.

The $i(V)$ curves comparing exact and WKB transmission currents are shown in figures 6 and 7. Figure 6 demonstrates the influence that the length of the barrier has on the transmission current, assuming a bare Au barrier. As expected the transmission currents for a short barrier, figure 6(a), are considerably larger than those in figure 6(b), for a long barrier. More importantly, figure 6(a) illustrates that the exact and WKB solutions diverge over the $\pm 2$ V bias voltage range. In addition, the exact current increases more rapidly compared to the WKB $i(V)$ curve. That is, the single dominant term in the WKB approximation is the square-root term (see equation (2)), while the higher-order terms in the Airy functions for the exact solution result in a rapid increase of the transmission function for the same range of bias voltage.

Figure 6(b), represents the 'far-field' calculation where the barrier length is 50 Å. In this case, the exact and WKB $i(V)$ curves are near-parallel and similar in value to each other. The WKB result mimics the asymptotic properties of the exact $i(V)$ curve. The WKB $i(V)$ curves provide some qualitative understanding, but are not a reliable description of the $i(V)$ curve for 'short' barrier lengths, i.e. $d < 30$–$50$ Å.

Figure 7 clearly demonstrates the difference between the exact and WKB $i(V)$ curves for both single and double trapezoidal barriers assuming a DEB molecule. Qualitatively, the two

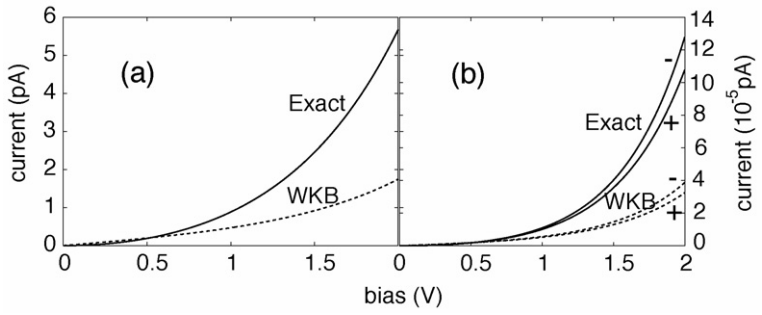


**Figure 7.** Exact and WKB barrier $i(V)$ curves for single and double trapezoidal barriers, respectively: (a) symmetrical $i(V)$ curves for DEB 9 Å in length; (b) asymmetrical $i(V)$ curves consisting of DEB, 9 Å, and a gap of 5 Å.

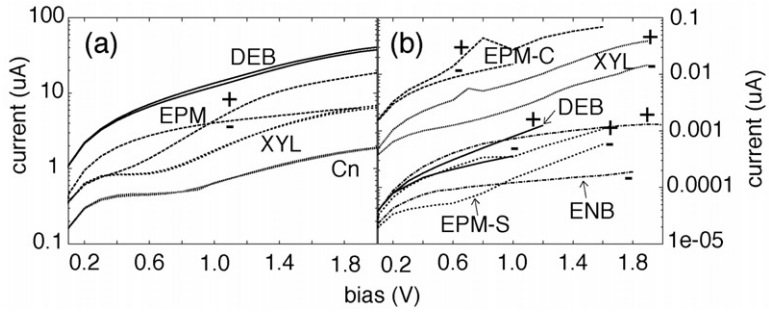


**Figure 8.** TranSIESTA calculated $i(V)$ curves with the molecules (a) spanning the interelectrode distance and (b) a 5 Å gap between the molecule and right electrode.

approaches are similar, in that for the single trapezoidal barrier the $i(V)$ curves are symmetric, while for the double barrier they are asymmetric, with reverse bias producing a larger current. In both cases, the currents for the exact result are ∼3–4 times larger at ±2 V compared to the WKB results. The magnitudes of the asymmetry between the reverse and forward biases at 2 V (or rectification) for both the exact and WKB double trapezoidal models are approximately equal at about 19% increase.

### *3.4. i(V) curves using density functional theory*

Figure 8 shows the $i(V)$ curves calculated with the TranSIESTA-C software package: in figure 8(a) the molecule spans the interelectrode region and in figure 8(b) there is a 5 Å gap between the terminating sulfur/carbon atom and the right gold surface. For ENB the 5 Å gap was measured between the gold electrode and the nitrogen atom. A measurement to the oxygen atoms increases the overall interelectrode distance by about 1–14.3 Å, in closer agreement with the other molecular systems. However, this reduces the conductance by three orders of magnitude. Although this behaviour makes comparisons difficult, we point out that the interelectrode distance for the ENB result in figure 8(b) is shorter than in the other cases. This points to a lower conductance for ENB than its counterparts with the same ethynyl linker on the left electrode, but different endgroups on the gap side. The same result is obtained in the tunnel barrier model where the surface work function is increased by ENB due to the inherent dipole moment of the molecule.

Figure 8(b) shows the large asymmetry in the $i(V)$ curves predicted by the DFT–NEGF theory with rectification of almost an order of magnitude. This is much more pronounced than in the tunnel barrier results. For all molecules a larger current is calculated when electrons are flowing from left to right, i.e. first through the molecule and then through the gap. For all but the ENB molecule this is opposite to the direction of larger transmission predicted by the tunnel barrier model.

In order to obtain a sensible comparison between the $i(V)$ curves for the different molecules shown in figure 8(a) it is important that their lengths be similar. This is true for DEB, EPM and XYL, but hexanedithiol (C6) is somewhat longer. We have therefore calculated the $i(V)$ curves for butanedithiol (C4) and C6, and interpolated between the two to obtain a representative $i(V)$ curve for the alkanedithiol family which is similar in length to the other molecules (denoted by Cn in figure 8(a)). As expected the current for the alkanedithiol is smaller than for the aromatic molecules XYL, EPM and DEB. This is because the alkane chains have more localized orbitals and are considered 'molecular insulators'. Comparing the three aromatic molecules, we see that the current for EPM lies in between that for XYL and DEB. This is a sensible result, since EPM has one ethynyl end the same as in DEB and one thiol end the same as in XYL. The fact that the current for DEB is so much larger than XYL, can be attributed to two factors, both discussed in [19]: the ethynyl–gold bond has larger interaction energy than the thiol–gold bond; and the conjugation in DEB is not broken by the presence of a thiol linker as in the XYL case but continues all the way through the molecule directly to the surface gold atoms.

Note the non-trivial behaviour of the $i(V)$ curve of EPM in figure 8(a): the asymmetry reverses at a bias of about 1 V. Below 1 V the asymmetry corresponds to the tunnel barrier case. Again the asymmetry is much more pronounced in the DFT–NEGF results than the tunnel barrier results.

Comparing figure 8(a) with figures 4(a) and 7(a) reveals that the DFT–NEGF currents are about five to six orders of magnitude larger than the tunnel barrier currents. The geometries used in the DFT calculations are idealized, and as pointed out in the introduction this is known to lead to an overestimation of the current. Comparison with experiment is not trivial due to the large spread in experimental data, which, as pointed out by Akkerman *et al* [35], may be as large as seven orders of magnitude. Our tunnel barrier currents are very similar in size to that reported in [35] for decanedithiol. However, that molecule is about 17 Å in length, and for a molecule that long our tunnel barrier currents would be about seven orders of magnitude smaller.

At a bias of 1 V, the heights of the barriers in the tunnelling model that would yield currents matching those calculated with DFT–NEGF are 0.63, 0.48, 0.35 and 0.12 eV for C6, XYL, EPM and DEB, respectively. This points to a more complicated picture than lowering of the surface work function.

## 4. Conclusion

In this paper we have compared the $i(V)$ curves using the WKB approximation, exact solution of time-independent Schrödinger equation and density functional non-equilibrium Green's functions (DFT–NEGF) for a range of symmetrical and non-symmetrical single molecules. The results presented encompass the full range of static techniques currently available. The WKB approximation is one extreme, whereby qualitative and phenomenological understanding of the molecules is obtained; the exact solution of the Schrödinger equation sits in the middle, providing a phenomenological understanding based upon an exact approach, while DFT–NEGF is at the other extreme, whereby a full quantitative understanding of the electronics of molecules can be developed.

In order to obtain barrier heights for the tunnelling model, we have made highly accurate DFT calculations of the surface work function of bare Au(111) and with various adsorbed molecules. Our value for bare Au(111) of 5.13 eV compares well with the experimental value of 5.31 eV. The adsorption of thiol and ethynyl linkers is seen to reduce the work function, the latter being more effective. Adsorption of 1-ethynyl-4-nitrobenzene (ENB) increases the work function due to the inherent dipole moment of the molecule.

The exact and WKB results are qualitatively consistent with each other. Both methods predict that rectification can be induced by non-symmetrical molecules, or by including a small air gap in between the molecule and the electrode. In either case, the effect is to introduce a barrier of different height at the two electrodes. The WKB method was used to explore the influence of a rounded trapezoidal barrier on the $i(V)$ curves in order to simulate image charge effects. The magnitude of the tunnelling current and asymmetry between the forward and reverse biases are both increased by introducing a rounded barrier.

On the other hand, quantitatively the two methods yield considerably different $i(V)$ curves. This difference is reflected in both the curvature of the $i(V)$ plots, where the exact solution predicts a much faster rate of increase of current with applied bias, and the absolute magnitude of the tunnelling currents, where again the exact solution gives larger currents. The magnitude of rectification at the maximum bias voltage is similar $\sim$20% for both methods. This result demonstrates that care has to be taken when using the WKB method to calculate tunnelling currents, particularly for tunnel junctions shorter than about 30–50 Å. For larger tunnel junctions the WKB method gives a reliable approximation to the true solution, at least over modest bias voltages.

The DFT–NEGF results include the entire electronic structure of the molecular system, and therefore more detailed phenomenological information may be expected. Comparing the absolute values of the $i(V)$ plots for different molecules, the dominating factor is apparently the degree of conjugation of the molecular orbitals: alkane chains are the least conductive and aromatic molecules linked to the gold electrodes via carbon–carbon triple bonds (DEB) are more conductive than those with thiol linkers (XYL). This result suggests that ethynyl linkers could provide an important new class of SAMs for molecular electronics. The latter ordering is to some degree captured by the tunnel barrier model, where the tunnelling current is dominated by the work function, since the carbon–gold bond is seen to reduce the surface work function by a greater amount than the sulfur–gold bond. In all cases there is a significant difference between currents calculated with the DFT–NEGF method and the tunnel barrier method. The former typically gives currents in the $\mu$A, while the latter is in the pA regime.

The DFT–NEGF results for the systems with a gap between the molecule and right electrode are difficult to interpret due to the high sensitivity to the interelectrode distance (i.e. the exact length of the gap). This sensitivity may be addressed in future by increasing the accuracy of the calculations, in particular reducing the orbital confinement. However, we believe that the results point to the ENB molecule being less conductive than its counterparts, similar to the tunnel barrier prediction.

The DTF–NEGF calculations predict significant asymmetry in the $i(V)$ characteristics of the molecule–gap geometries; up to an order of magnitude in the case of ENB. Furthermore, the current is consistently larger for forward bias, i.e. electron transport from the molecule side to the gap side. The opposite asymmetry is predicted by the tunnel barrier model. This result is, in principle, easy to verify experimentally as the geometry reflects a realistic situation in STM experiments. Significant rectification in such a simple system is highly desirable from the point of view of device fabrication. The $i(V)$ characteristic of the inherently asymmetric EPM molecule is interesting in that the asymmetry between forward and reverse bias currents inverts at 1 V. Asymmetry of up to a factor of two is predicted.

Absolute values of the static DFT tunnelling currents may well be reduced by inclusion of dynamic effects, as shown by Sai *et al* [10], bringing them closer to the currents predicted by our tunnel barrier models. The dynamic correction depends upon the change in charge distribution across the junction. The organic molecules investigated here are expected to be quite covalently bound to the gold electrodes [19, 36] and therefore give rise to a relatively slowly varying charge distribution. By contrast the vacuum gaps might be expected to lead to larger dynamic corrections. The asymmetry predicted in our static DFT calculations will, presumably, be preserved by the inclusion of these dynamic effects, although clearly a full dynamic calculation is required to clarify this.

A combination of the techniques employed in this work can provide important insights into the design of molecular electronics. Barrier model techniques (i.e. WKB and exact) enable a phenomenological understanding of the $i(V)$ properties of molecules in terms of multi-trapezoidal barrier models at very modest computational expense. Using information gained from this phenomenological modelling, the DFT–NEGF-based techniques can be used to explore the $i(V)$ and conductance properties of the designer molecule by employing full quantum mechanical calculations, at considerable computational cost. This approach to design and processing enables nanotechnology to step toward fully functional nanodevices, in which the present and future limitations in silicon-based technology can be addressed.

## References


[1] Aviram A and Ratner M A 1974 *Chem. Phys. Lett.* **29** 277
[2] Kohn W and Sham L J 1965 *Phys. Rev.* **140** A1133
[3] Hohenberg P and Kohn W 1964 *Phys. Rev.* **136** B864
[4] Stokbro K, Taylor J, Brandbyge M, Mozos J L and Ordejon P 2003 *Comput. Mater. Sci.* **27** 151
[5] Pontes R B, Novaes F D, Fazzio A and da Silva A J R 2006 *J. Am. Chem. Soc.* **128** 8996
[6] Muller K H 2006 *Phys. Rev.* B **73** 045403
[7] Hu Y B, Zhu Y, Gao H J and Guo H 2005 *Phys. Rev. Lett.* **95** 156803
[8] Hoft R C, Liu J, Cortie M B and Ford M 2006 *Proc. SPIE: BioMEMS and Nanotechnology II* vol 6036, ed D V Nicolau, p 603603
[9] Hoft R C, Ford M and Cortie M B 2006 *Chem. Phys. Lett.* **429** 503
[10] Sai N, Zwolak M, Vignale G and Di Ventra M 2005 *Phys. Rev. Lett.* **94** 18610
[11] Bushong N, Sai N and Di Ventra M 2005 *Nano Lett.* **5** 2569
[12] Di Ventra M and Todorov T N 2004 *J. Phys.: Condens. Matter* **16** 8025
[13] Gorodetsky D A and Melnik Y P 1977 *Surf. Sci.* **62** 647
[14] Cortenraad R, van der Gon A W D, Brongersma H H, Gartner G and Manenschijn A 2002 *Appl. Surf. Sci.* **191** 153
[15] Soler J M, Artacho E, Gale J D, Garcia A, Junquera J, Ordejon P and Sanchez-Portal D 2002 *J. Phys.: Condens. Matter* **14** 2745
[16] Ordejon P, Artacho E and Soler J M 1996 *Phys. Rev.* B **53** 10441
[17] Troullier N and Martins J L 1991 *Phys. Rev.* B **43** 1993
[18] Monkhorst H J and Pack J D 1976 *Phys. Rev.* B **13** 5188
[19] Ford M J, Hoft R C and McDonagh A 2005 *J. Phys. Chem.* B **109** 20387
[20] Perdew J P, Burke K and Ernzerhof M 1996 *Phys. Rev. Lett.* **77** 3865
[21] Hoft R C, Gale J D and Ford M 2006 *Mol. Sim.* **32** 593
[22] Brandbyge M, Mozos J L, Ordejon P, Taylor J and Stokbro K 2002 *Phys. Rev.* B **65** 165401
[23] Perdew J P and Zunger A 1981 *Phys. Rev.* B **23** 5048
[24] Datta S 2005 *Quantum Transport: Atom to Transistor* (Cambridge: Cambridge University Press)
[25] Cortie M B, Zareie M H, Ekanayake S R and Ford M J 2005 *IEEE Trans. Nanotechnol.* **4** 406
[26] Bransden B H and Joachain C J 1989 *Introduction to Quantum Mechanics* (London: Longman) p 399
[27] Love J C, Estroff L A, Kriebel J K, Nuzzo R G and Whitesides G M 2005 *Chem. Rev.* **105** 1103
[28] Yourdshahyan Y, Zhang H K and Rappe A M 2001 *Phys. Rev.* B **63** 081405(R)
[29] Yourdshahyan Y and Rappe A M 2002 *J. Chem. Phys.* **117** 825
[30] Vitos L, Ruban A V, Skriver H L and Kollar J 1998 *Surf. Sci.* **411** 186

[31] Crljen Z, Lazic P, Sokcevic D and Brako R 2003 *Phys. Rev.* B **68**
[32] Boettger J C 1994 *Phys. Rev.* B **49** 16798
[33] Tyson W R and Miller W A 1977 *Surf. Sci.* **62** 267
[34] Lide D R (ed) 2006 *CRC Handbook of Chemistry and Physics* vol 87 (Boca Raton, FL: CRC Press) section 12, p 114
[35] Akkerman H B, Blom P W M, de Leeuw D M and de Boer B 2006 *Nature* **441** 69
[36] Ford M J, Masens C and Cortie M B 2006 *Surf. Rev. Lett.* **13** 297